Second Order Sliding Mode Controller Design for Pneumatic Artificial Muscle

Ammar Al-Jodah
Assistant Lecturer
Control and Systems Eng. Dep.
University of Technology, Baghdad- Iraq
ammar.aljodah@gmail.com

Laith Khames
Assistant Lecturer
Control and Systems Eng. Dep.
University of Technology, Baghdad- Iraq
laithkhames@yahoo.com

ABSTRACT

In this paper, first and second order sliding mode controllers are designed for a single link robotic arm actuated by two Pneumatic Artificial Muscles (PAMs). A new mathematical model for the arm has been developed based on the model of large scale pneumatic muscle actuator model. Uncertainty in parameters has been presented and tested for the two controllers. The simulation results of the second-order sliding mode controller proves to have a low tracking error and chattering effect as compared to the first order one. The verification has been done by using MATLAB and Simulink software.

Keywords: PAM, Sliding Mode Controller.

تصميم متحكم منزلق النمط من الدرجة الثانية لعضله اصطناعية هوائية

عمار الجوده
مدرس مساعد
قسم هندسة السيطرة و النظم
الجامعة التكنولوجية, بغداد-العراق

ليث خميس
مدرس مساعد
قسم هندسة السيطرة و النظم
الجامعة التكنولوجية, بغداد-العراق

الخلاصة

في هذه الورقة تم تصميم مسيطرين منزلقين النمط ذوي الرتبه الاولى و الثانيه للسيطرة على ذراع روبوتيه تدار بواسطة اثنين من العضلات الاصطناعية الهوائية. وقد تم تطوير نموذج رياضي جديد للذراع على أساس نموذج العضله الهوائية الضخمه. تم اختبار المسيطرين بعد الاخذ بعين الاعتبار عدم اليقين في المعاملات. المحاكاة اثبتت ان المسيطر المنزلق ذو الرتبه الثانيه يمتلك نسبة خطأ تتبع منخفضة و كذلك نسبة تأثير الثرثرة منخفضه بالمقارنة مع المسيطر المنزلق ذو الرتبه الاولى. تم التحقق باستخدام برنامج ماتلاب و سيمولينك.

الكلمات الرئيسية: عضلة اصطناعية هوائية , متحكم الانزلاق.

1. INTRODUCTION

In the past few years, Pneumatic Artificial Muscles (PAMs) has received great attention in the robotics industry for its compact size and high power. Robots are basically exoskeletons with actuators that provide the motion through torque and forces on the joints. Actuators are normally DC or AC motors, hydraulic or pneumatic cylinders. Despite the many advantages of these actuators, there is still a need for an actuator which is compact, flexible and has the ability to deliver higher power. Higher power applications required electric or hydraulic power to move, but pneumatics still have the potential to deliver high power with a compact design. For many years, the Pneumatic actuators were limited in the simple, repetitive tasks with a low level of automation. Pneumatic actuators were not adapted to be used in robotic systems very easily, the mean two obstacles were: 1- Pneumatic systems required complex controllers to achieve a high accuracy. 2- compliance (not robust to load variations). Air compressibility is the prime reason for those obstacles, **Caldwell, et al., 1995.**

PAMs overtake the main obstacles mentioned earlier since these PAMs has all the advantages of pneumatic actuators such as the low cost and compactness, and it does not have the disadvantages of low power and lack of compliance. Such light weight actuators have a great benefit in robotic systems since it will not greatly affect the payload. **Tondu, and Lopez, 2000**

A PAM is simply a cylinder made of a flexible rubber which fits inside a helical braided plastic sheath, **Ching-Ping Chou, and Hannaford, 1996**. This structure makes the PAM widened and shortened when its cylinder inflated. When PAM shorten it deliver high axel force as compared to its weight. The way PAM construction make it very similar to its human counterpart in the extent of its size and force.

Controlling PAM is a very challenging task since PAMs are continuously changing in shape, size, internal pressure, temperature, and axel force. With all these changes it is hard to find an accurate model for the PAM. The nonlinear and robust control technique is highly favorable in controlling PAMs where no accurate model is presented. Several works has been done using those techniques which includes: backstepping control, **Carbonell, et al., 2001** , adaptive control, **Lilly, 2003** and the sliding mode control **Utkin, 1978** , **Carbonell, et al., 2001** , **Lilly, and Liang Yang, 2005** , **Van Damme, et al., 2007** , and **Boudoua, et al., 2015** .

Sliding mode controllers are in the leads of robust controllers that are able to overtake the model uncertainties and external disturbances. I this paper a new model of one link robotic arm actuated by two large scale PAMs is presented. The model of PAMs is augmented with the model of one link robotic arm to have the overall model. Sliding mode controller will be used to control the arm to follow the desired trajectory. Second order sliding mode controller is used to overcome the chattering effect.

This paper is arranged as follows. Section 2 contains the derivation of the mathematical model of one link arm actuated by PAMs in the bicep/tricep configuration. Section 3 presents the derivation of a sliding mode controller for the robotic arm. Section 4 presents simulation results of the control system with the first order and second order sliding mode controllers. Section 5 contains the conclusions.

2. THE MATHEMATICAL MODEL

In general, before any controller design, it is important to obtain a mathematical model for the system to be controlled which is the closest approximation of its true behavior. The system can then be analyzed, and the controller can be designed to meet the required performance. The single link robotic arm is shown in Fig. **1**. The equation of motion of the single link robotic arm is given by

$$(ml^2 + I)\ddot{q} + mgl\cos q = \tau \quad (1)$$

Where $q, \ddot{q}$ are the arm rotation angle and angular acceleration respectively, m is the mass at the end of the arm, l is the arm length, I is the arm moment of inertia, g is the gravitational acceleration, and τ is the torque required to rotate the arm. The torque is generated by the bicep and tricep PAMs and is given by the equation , **Lilly, and Liang Yang, 2005**:

$$\tau = (F_t(.) - F_b(.))r \quad (2)$$

Where $F_t(.)$ and $F_b(.)$ are the forces generated from the tricep and bicep PAMs respectively, r is the pully radius. The PAM model given by **Repperger, et al., 1998,** is used to find $F_t(.)$ and $F_b(.)$ as follows

$$F_t(.) = -K_t(x_t)x_t - B_t(\dot{x_t})\dot{x_t} + P_t \quad (3)$$

$$F_b(.) = -K_b(x_b)x_b - B_b(\dot{x_b})\dot{x_b} + P_b \quad (4)$$

Where $K_t(x_t), K_b(x_b)$ is the tricp and bicep PAM spring coeffecients respectively. These coeffecients are nonlinear function of PAM postion. $B_t(\dot{x_t}), B_b(\dot{x_b})$ is the tricp and bicep PAM damper coeffecients respectively. These coeffecients are nonlinear function of PAM velocity. x_t, x_b are the amount of PAM contraction for tricep and bicep respectively. $\dot{x_t}, \dot{x_b}$ are the velocity of PAM contraction for tricep and bicep respectively. P_t, P_b are the pressure of tricep and bicep PAMs respectively. The $K_i(x_i), B_i(\dot{x_i})$, where $i = (b, t)$ is given by **Repperger, et al., 1998**:

$$K_i(x_i) = k_{1i}x_i^2 + k_{2i}x_i + k_{3i} \qquad i = (b, t) \quad (5)$$

$$B_i(\dot{x_\iota}) = b_{1i}\dot{x_\iota}^2 + b_{2i}\dot{x_\iota} + b_{3i} \qquad i = (b, t) \quad (6)$$

Where $k_{1i}, k_{2i}, k_{3i}, b_{1i}, b_{2i},$ and b_{3i} are constants given in **Table 1, Repperger, et al., 1998**. These constants takes two states, one when the PAM inflated and the other one when it is deflated. The bicep and tricep PAM state is given by

$$\dot{q} < 0 \Rightarrow \begin{cases} bicep\ inflated \\ tricep\ deflated \end{cases}$$
$$\dot{q} > 0 \Rightarrow \begin{cases} bicep\ deflated \\ tricep\ inflated \end{cases} \quad (7)$$

The pressure of tricep and tricep PAM is given by

$$P_t = P_{0t} + \Delta P \quad (8)$$

$$P_b = P_{0b} + \Delta P \quad (9)$$

Where P_{0t}, P_{0b} are the initial pressure of the tricep and bicep respectively, ΔP is the pressure difference between the tricep and bicep respectively. ΔP is the control input to the system. The amount of muscle contraction x_t, x_b is given by **Lilly, and Liang Yang, 2005**:

$$x_t = \left(\frac{\pi}{2} + q\right)r, \dot{x}_t = r\dot{q} \quad (10)$$

$$x_b = \left(\frac{\pi}{2} - q\right)r, \dot{x}_b = -r\dot{q} \quad (11)$$

Where the angle $\frac{\pi}{2}$ is considered as the zero position at which both x_t and x_b is zero.

By substituting Eq. (8) and Eq. (9) in Eq. (3) and Eq. (4), after that substituting in Eq. (2) gives

$$\tau = (-K_t(x_t)x_t - B_t(\dot{x}_t)\dot{x}_t + P_{0t} + \Delta P + K_b(x_b)x_b + B_b(\dot{x}_b)\dot{x}_b - P_{0b} + \Delta P\ )r \quad (12)$$

By substitute Eq. (5) and Eq. (6) in Eq. (12)

$$\begin{aligned}\tau = \big(&-(k_{1t}x_t^2 + k_{2t}x_t + k_{3t})x_t - (b_{1t}\dot{x}_t{}^2 + b_{2t}\dot{x}_t + b_{3t})\dot{x}_t + P_{0t} + \Delta P \\ &+ (k_{1b}x_b^2 + k_{2b}x_b + k_{3b})x_b + \big(b_{1b}\dot{x}_b{}^2 + b_{2b}\dot{x}_b + b_{3b}\big)\dot{x}_b - P_{0b} \\ &+ \Delta P\ \big)r\end{aligned} \quad (13)$$

By substituting Eq. (10) and Eq. (11) in Eq. (13) and the result in Eq. (1) gives

$$\left.\begin{gathered}\ddot{q} = \delta_1 q^3 + \delta_2 q^2 + \delta_3 q + \delta_4 \dot{q}^3 + \delta_5 \dot{q}^2 + \delta_6 \dot{q} + \delta_7 \cos q + \delta_8 + bu \\ u = \Delta P \\ \delta_1 = \frac{-r^3(k_{1b} + k_{1t})}{ml^2 + I} \\ \delta_2 = \frac{\frac{3\pi r^4}{2}(k_{1b} - k_{1t}) + r^3(k_{2b} - k_{2t})}{ml^2 + I} \\ \delta_3 = -\frac{(3\pi r^4/2)(k_{1b} - k_{1t}) + \pi r^3(k_{2b} + k_{2t}) + r^2(k_{3b} + k_{3t})}{ml^2 + I} \\ \delta_4 = \frac{-r^4(b_{1b} + b_{1t})}{ml^2 + I} \\ \delta_5 = \frac{r^3(b_{2b} - b_{2t})}{ml^2 + I} \\ \delta_6 = \frac{-r^2(b_{3b} - b_{3t})}{ml^2 + I} \\ \delta_7 = -\frac{glm}{ml^2 + I} \\ \delta_8 = -\frac{r(P_{0b} - P_{0t}) + \frac{\pi r^4}{8}(k_{1t} - k_{1b}) + \frac{\pi r^3}{4}(k_{2t} - k_{2b}) + \frac{\pi r^2}{2}(k_{3t} - k_{3b})}{ml^2 + I} \\ b = \frac{2r}{ml^2 + I}\end{gathered}\right\} \quad (14)$$

The robotic arm parameters are assumed as in **Table 2**.
To consider the uncertainty, the system is represented as following

$$\left.\begin{gathered}\ddot{q} = f_0 + \Delta f + bu \\ f_0 = \delta_1 q^3 + \delta_2 q^2 + \delta_3 q + \delta_4 \dot{q}^3 + \delta_5 \dot{q}^2 + \delta_6 \dot{q} + \delta_7 \cos q + \delta_8 \\ \Delta f = \Delta\delta_1 q^3 + \Delta\delta_2 q^2 + \Delta\delta_3 q + \Delta\delta_4 \dot{q}^3 + \Delta\delta_5 \dot{q}^2 + \Delta\delta_6 \dot{q} + \Delta\delta_7 \cos q + \Delta\delta_8\end{gathered}\right\} \quad (15)$$

Where the nominal values $\delta_i, i = 1,2,\dots,8$ are given in **Table 3** which obtained by substituting the parameters of **Table 1** and **Table 2** in Eq. (14).
The uncertainty parameters $\Delta\delta_i, i = 1,2,\dots,8$ is a percentage of the nominal values.

3. SLIDING MODE CONTROLLER DESIGN

The task in sliding mode controller design is to find a function of states called sliding function and a state-feedback control law $u\big(x(t)\big) = u_{eq} + u_{sw}$. The control law will drive the state towards the sliding surface (reaching phase), and then makes it slide on it to origin $x = [0 \quad 0 \quad ... \quad 0 \quad]^T$ (sliding phase). If the states were the error and its derivatives, then a tracking behavior can be ensured if the states return to origin, **Utkin, et al., 2009** . The reaching condition is given by $s\dot{s} < 0$, which is satisfied by the switching part of the control action u_{sw}. The sliding condition is to maintain $s = 0$, which is satisfied by the equivalent part of the control action u_{eq}. The error equation is given by

$$e = q - q_d \tag{16}$$

Where q_d is the desired angle. Diffrentiate Eq. (16) gives

$$\dot{e} = \dot{q} - \dot{q}_d \tag{17}$$

The second derivative of Eq. (17) gives

$$\ddot{e} = \ddot{q} - \ddot{q}_d \tag{18}$$

Define the surface function as following

$$s = \dot{e} + \lambda e \tag{19}$$

The derivative of the surface function is given by

$$\dot{s} = \ddot{e} + \lambda \dot{e} \tag{20}$$

By substituting Eq. (18) in Eq. (20) gives

$$\dot{s} = \ddot{q} - \ddot{q}_d + \lambda \dot{e} \tag{21}$$

By substituting Eq. (15) in Eq. (21) gives

$$\dot{s} = f_0 - \ddot{q}_d + \lambda \dot{e} + \Delta f + bu \tag{22}$$

The proposed control law is given by

$$u = \frac{1}{b}\left(u_{eq} + u_{sw}\right) \tag{23}$$

Where the proposed u_{eq} is

$$u_{eq} = -f_0 + \ddot{q}_d - \lambda \dot{e} \tag{24}$$

Substituting Eq. (24) in Eq. (23) then the result in Eq. (22) gives

$$\dot{s} = \Delta f + u_{sw} \tag{25}$$

Let $u_{sw} = -k\ sign(s)$, Eq. (25) becomes

$$\dot{s} = \Delta f - k\ sign(s) \tag{26}$$

The reaching condition $s\dot{s} \leq 0$ must be satisified as following

$$\begin{aligned} s\dot{s} &= s\Delta f - ks\ sign(s) \\ &= s\Delta f - k|s| \\ &\leq |s||\Delta f| - k|s| \\ &\leq -|s|(k - |\Delta f|) \end{aligned} \tag{27}$$

the above equation is true if the following condition hold

$$k > |\Delta f| \tag{28}$$

In this paper,it has been noted from simulation that selecting k as $k = 1$, will be enough to cancel out the uncertainties in the system. Choosing a value more than one will cause more chattering in the control action.

It is well known that the classical sliding mode controller has a high chattering in the control action. The chattering effect makes things difficult in the implementation because of the high frequency of on and off states which are never practical for the PAM system. To solve this problem, chattering reduction methods is used. One of the methods to reduce the chattering is to consider the second order sliding mode. In the second order sliding mode, the derivative of control action appears in the second derivative of the surface function which represents the virtual control as following, **Bartolini, et al., 2009**:

$$\ddot{s} = \varphi(t,x) + \gamma(t,x)\dot{u}$$

and the following conditions are assumed

$$|u| \le U_M$$
$$0 < \Gamma_m < \gamma(t,x) < \Gamma_M$$
$$|\varphi(t,x)| < \Phi$$

Where U_M, Γ_m, Γ_M, and Φ are positive constants. One of the efficient second order sliding mode algorithms is the super twisting algorithm. The super twisting controller is widely implemented in real-time applications for its high robustness and easy to implement properties. It can be seen as a nonlinear version of the classical PI controller. Super twisting is an algorithm developed specifically to control systems of relative degree one with the main advantage of chattering reduction. The trajectories of the 2-sliding exhibit a twisting motion around the origin, hence the name, see **Fig. 2**. The continuous control $u(t)$ has two terms. The first one is a continuous function of the sliding variable. The second one is an integration of a discontinuous first order differential equation. The control algorithm is defined by the following control law, **Bartolini, et al., 2009:**

$$\mathrm{u} = -\lambda|\mathrm{s}|^{\rho}\mathrm{sign}(s) + \int -\mathrm{W}\ \mathrm{sign}(s)dt \tag{29}$$

the convergence to the sliding manifold will be in finite time if the following sufficient conditions satisfied, **Bartolini, et al., 2009**:

$$W > \frac{\Phi}{\Gamma_m}$$
$$\lambda^2 \ge \frac{4\Phi}{\Gamma_{\mathrm{m}}^2}\frac{\Gamma_M(W+\Phi)}{\Gamma_m(W-\Phi)} \tag{30}$$
$$0 < \rho \le 0.5$$

From Eq. (25), differentiate $\dot{s}$ again to get

$$\ddot{\mathrm{s}} = \Delta\dot{f} + \dot{u}_{sw} \tag{31}$$

From Eq. (31), $\gamma(t,x) = 1$, $\varphi(t,x) = \Delta\dot{f}$, both are bounded. These conditions $0 < \Gamma_m < \gamma(t,x) < \Gamma_M$ and $|\varphi(t,x)| < \Phi$ are satisfied since both $\gamma(t,x)$ and $\varphi(t,x)$ are bounded, however, finding an exact value for $\Gamma_m, \Gamma_M, and\ \Phi$ is difficult. But however, The following values can be used for Γ_m and Γ_M: $\Gamma_m = 0.9$, $\Gamma_M = 1.1$. A conservative value of $\Phi = 0.5$ will be assumed since it is difficult to find an exact estimation. Parameters have to satisfy the following conditions: first condition $W > \left(\frac{\Phi}{\Gamma_m} = 0.5556\right)$ a value of $W = 1$ is chosen, second condition

$\lambda^2 \geq \left(\frac{4\Phi}{\Gamma_m^2}\frac{\Gamma_M(W+\Phi)}{\Gamma_m(W-\Phi)} = 3.6885\right) \Rightarrow \lambda \geq 1.9205$ a value of $\lambda = 2$ is chosen. And finally ρ chosen as $\rho = 0.5$.

4. SIMULATION RESULTS

The Classical Sliding Mode Control (CSMC) system is shown in **Fig. 3**. A smooth desired angle trajectory is used to test the proposed controllers given by **Lilly, and Liang Yang, 2005:**

$$q_d = \pi/2 + 0.5(\sin(2\pi \times 0.02t) + \sin(2\pi \times 0.05t) + \sin(2\pi \times 0.09t)) \quad (32)$$

The initial angle is $57.2958°$. The uncertainty in the parameters is taken as 5 percent. The sampling time has been chosen as 0.001 second. **Fig. 4** shows the desired and actual trajectory of the robot arm angle, it can be noted that the two trajectories are matched after few seconds of the initial position. **Fig. 5** shows the angular velocity of the Arm. It can be noted that the arm suffers from oscillation in the velocity which is comes from the chattering phenomena in the control action. **Fig. 6** shows the control action which has a high amount of chattering this is also apparent in torque in **Fig. 7**, in practice this control action cannot be implemented since there is no way to supply such pressure in this high frequency.

The Second Order Sliding Mode Control (SOSMC) system is shown in **Fig. 8**. The desired angle trajectory is given by Eq. 32. The initial angle is $57.2958°$. The uncertainty in the parameters is also taken as 5 percent. **Fig. 9** shows the angle response of the arm under SOSMC which is faster than the case of CMC. In **Fig. 10** the angular velocity does not suffer from any chattering, that can also be noted in the control action in **Fig. 11** and torque in **Fig. 12**.

In order to measure the effectiveness of the two controllers and make a clear performance comparison, a more aggressive reference command is used. A sudden change reference command is used to test the command following and chattering phenomena. The reference command is consisting of two steps, the first one is a step of $50°$ for the first twenty seconds, the second step is $150°$ and it start from the second 20 to the second 60 as in **Fig. 13**.

Fig. 13 shows that CSMC can follow the step command but with high overshoot, and that's perfectly fine because of the aggressive change in the reference command which induce high error in the controller making it produce high control action. The velocity of CSM is shown in **Fig. 14** where a chattering can be seen. The control action and torque in **Fig. 15** and **Fig.16** respectively shows a high amount of chattering. **Fig. 17** shows the phase plane of the closed loop system, the system starts at the initial condition where $e = 1$ and $\dot{e} = 0$, then it start the reaching phase as can be seen as a half circle below the surface line (the blue line) then it hits the surface line and slide along it to the zero. When the second step happen the system state jumps from zero and enter the reaching phase again as can be seen as the upper half circle then it hits the surface line and slide along it to the zero. It can be noticed the chattering happening in the sliding phase when the states move along $s = 0$. In **Fig. 18** it can be noticed the surface function has a sudden jump at the start of each step and it reach zero after around three seconds.

In SOSMC the angle response is shown in **Fig. 19** where the angle follows the desired command with high overshoot similar to the case of CSMC. In **Fig. 20** the velocity does not suffer from any chattering. The control action and torque are shown in **Fig. 21** and **Fig. 22** respectively, both does not have chattering and the curves appear like a filtered version of the case of CSMC, that's because the Signum function is appeared under the integration operator. The phase plane in **Fig. 23** does not show any chattering and the states slide smoothly in the sliding phase. The surface function curve is shown in **Fig. 24**, the surface function requires

around four seconds to reach zero from the sudden jump, which is a one second more in case of CSMC, this increase in time comes with chattering free unlike the case of CSMC.

5. CONCLUSIONS

In this work, a single link robotic arm actuated by a large scale pneumatic muscle actuator has been studied and explained. A new mathematical model has been developed for this system which has not been developed in pervious researches. This robotic arm suffers from uncertainties in the parameters, these uncertainties comes from the compressibility of the air. In order to have an accurate position tracking, a robust control algorithm is needed. A classical sliding mode controller has been desired as a first step to control the system. It has been noted that this type of controller has a high chattering in the control action which make it impractical to implement in a real system. To mitigate this problem. A second order sliding mode controller is designed. In this controller the term responsible of the chattering phenomena is integrated. The integration operation reduces the chattering greatly and that has been showed in the results.

REFERENCES

- Bartolini, G., Pisano, A. and Usai, E., 2009. *On The Second-Order Sliding Mode Control of Nonlinear Systems With Uncertain Control Direction*. Automatica, Vol. 45, No. 12, pp.2982–2985.

- Boudoua, S., Hamerlain, M. and Hamerlain, F., 2015. *Intelligent Twisting Sliding Mode Controller Using Neural Network for Pneumatic Artificial Muscles Robot Arm*. In 2015 International Workshop on Recent Advances in Sliding Modes (RASM). IEEE, pp. 1–6.

- Caldwell, D.G., Medrano-Cerda, G.A. and Goodwin, M., 1995. *Control of Pneumatic Muscle Actuators*. IEEE Control Systems, Vol. 15, No. 1, pp.40–48

- Carbonell, P., Jiang, Z.P. and Repperger, D.W., 2001. *Nonlinear Control of A Pneumatic Muscle Actuator: Backstepping Vs. Sliding-Mode*. In Proceedings of the 2001 IEEE International Conference on Control Applications (CCA'01) , pp. 167–172.

- Ching-Ping Chou and Hannaford, B., 1996. *Measurement and Modeling of Mckibben Pneumatic Artificial Muscles*. IEEE Transactions on Robotics and Automation, Vol. 12 No. 1, pp.90–102.

- Van Damme, M. et al., 2007. *Proxy-Based Sliding Mode Control of a Manipulator Actuated by Pleated Pneumatic Artificial Muscles*. In Proceedings 2007 IEEE International Conference on Robotics and Automation, pp. 4355–4360.

- Lilly, J.H., 2003. *Adaptive Tracking for Pneumatic Muscle Actuators in Bicep and Tricep Configurations*. IEEE Transactions on Neural Systems and Rehabilitation Engineering, Vol. 11 No. 3, pp.333–339.

- Lilly, J.H. and Liang Yang, 2005. *Sliding Mode Tracking for Pneumatic Muscle Actuators in Opposing Pair Configuration*. IEEE Transactions on Control Systems Technology, Vol. 13 No. 4, pp.550–558.

- Repperger, D.W., Johnson, K.R. and Phillips, C.A., 1998. *A VSC Position Tracking System Involving a Large Scale Pneumatic Muscle Actuator*. In Proceedings of the 37th IEEE Conference on Decision and Control, pp. 4302–4307.

- Tondu, B. and Lopez, P., 2000. *Modeling and Control of Mckibben Artificial Muscle Robot Actuators*. *IEEE Control Systems Magazine*, Vol. 20, No 2, pp.15–38.

- Utkin, V., Guldner, J. and Shi, J., 2009. *Sliding Mode Control in Electro-Mechanical Systems*, 1st edition, Florida, United States, CRC Press.

- Utkin, V.I., 1978. *Sliding Modes and their Application in Variable Structure Systems*. 1st edition, Moscow, Russia, MIR Publishers.

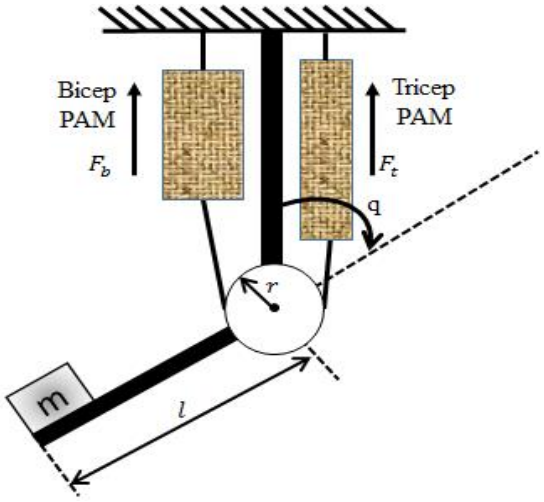

Figure 1. Single link robotic arm actuated by PAMs.

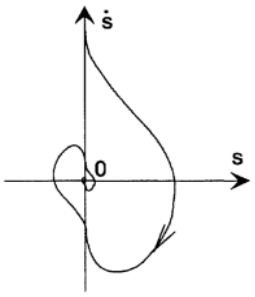

Figure 2. Super-twisting algorithm phase trajectory.

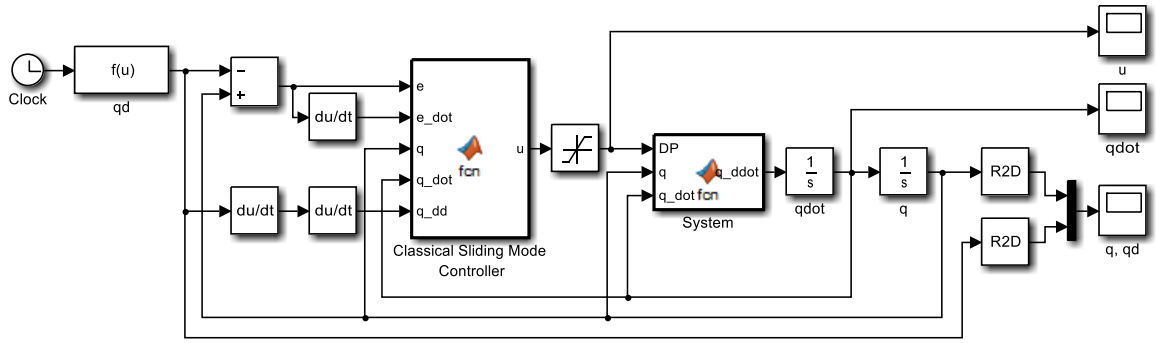

Figure 3. Classical sliding mode control system Simulink.

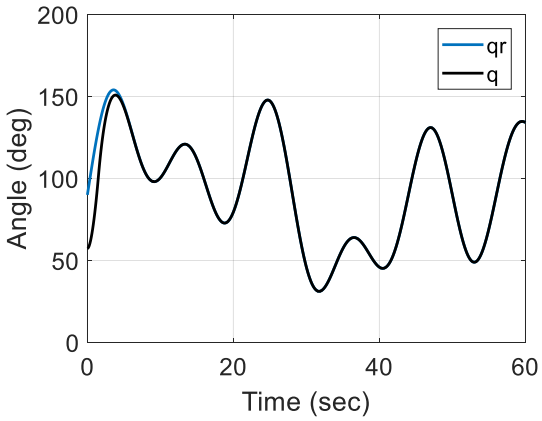

Figure 4. Angle response of CSMC.

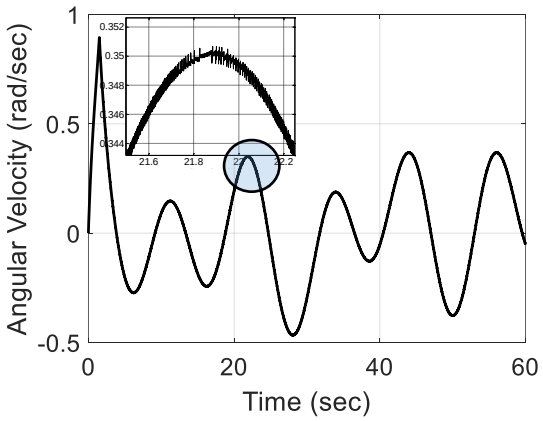

Figure 5. Angular velocity response of CSMC.

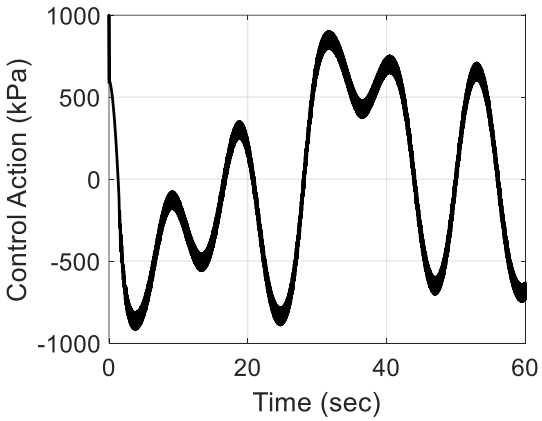

Figure 6. Control action of CSMC.

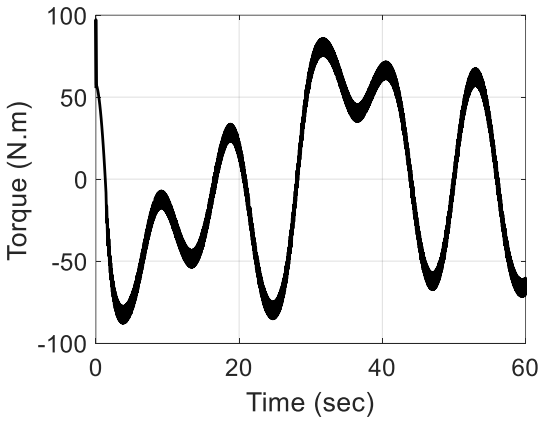

Figure 7. Torque of CSMC.

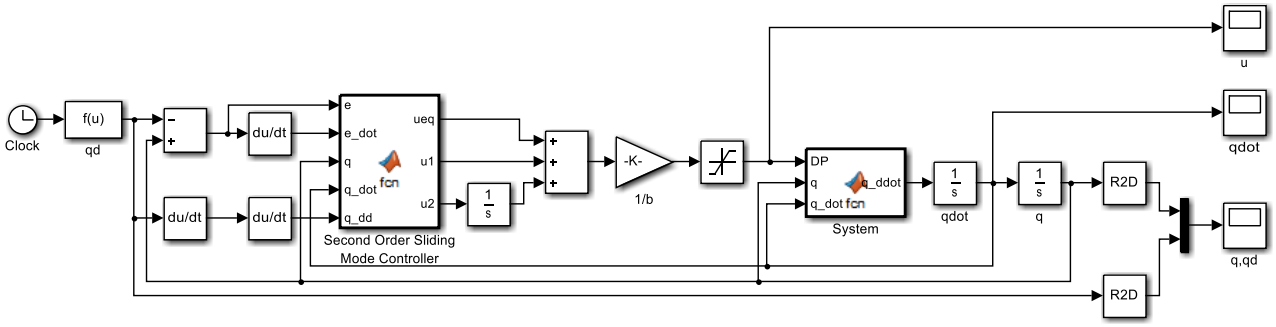

Figure 8. Second order sliding mode control system Simulink.

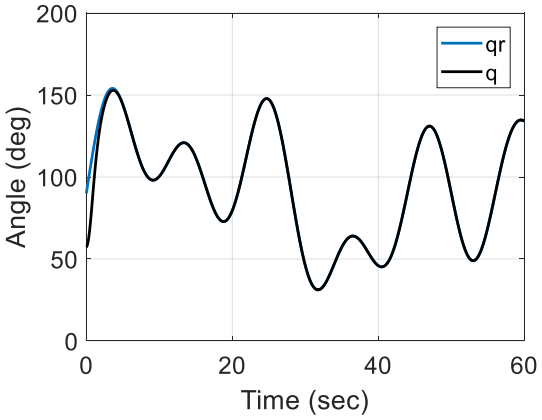

Figure 9. Angle response of SOSMC.

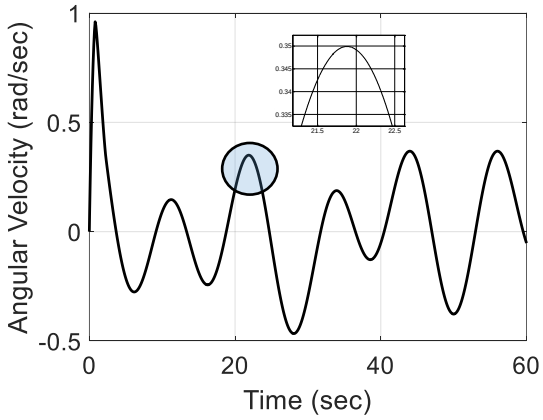

Figure 10. Angular velocity response of SOSMC.

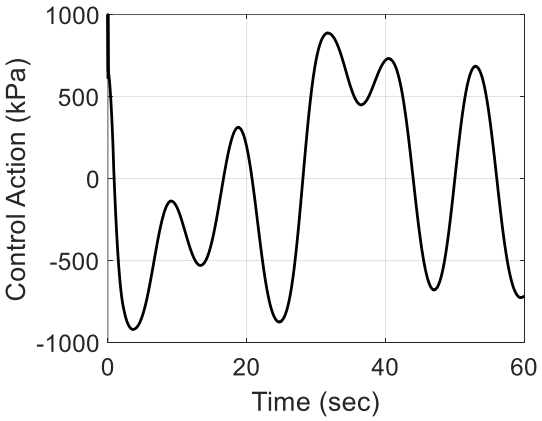

Figure 11. Control action of SOSMC.

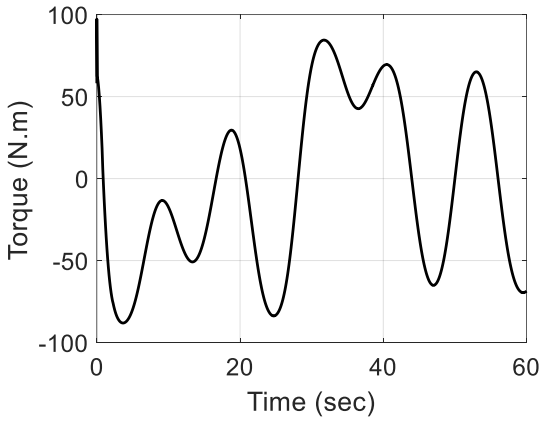

Figure 12. Torque of SOSMC.

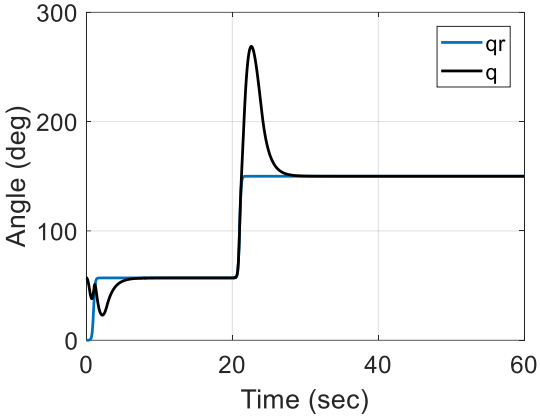

Figure 13. Angle response of CSMC for step command.

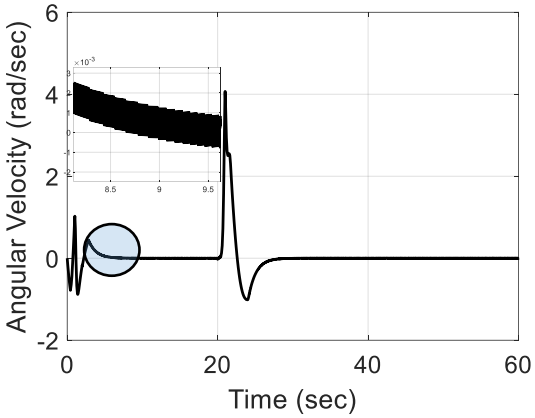

Figure 14. Angular velocity response of CSMC for step command.

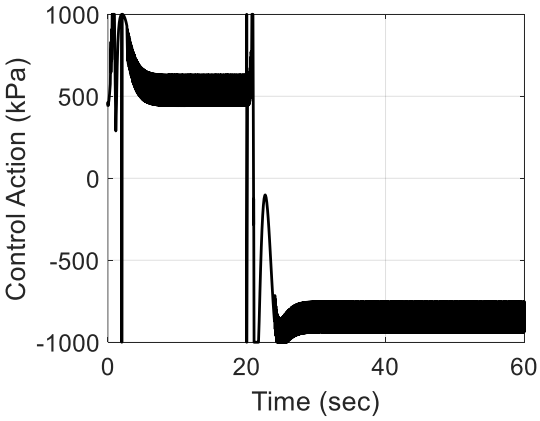

Figure 15. Control action of CSMC for step command.

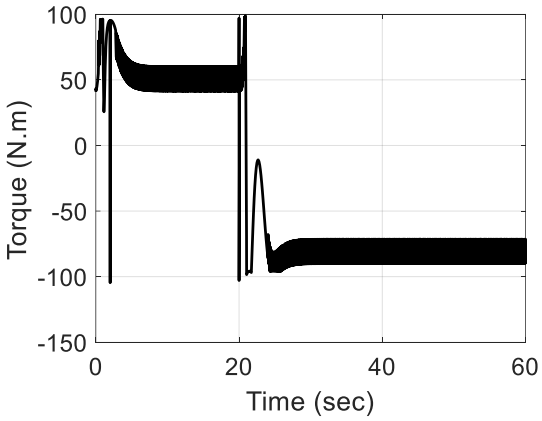

Figure 16. Torque of CSMC for step command.

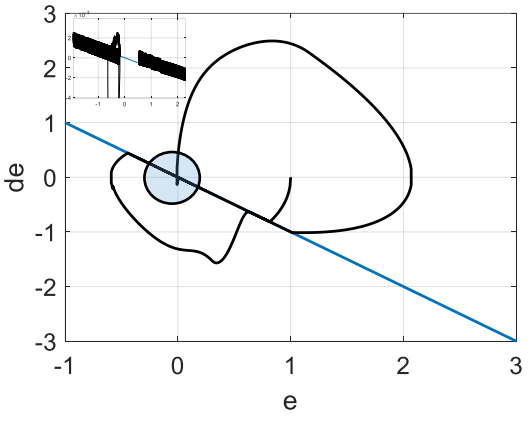

Figure 17. Phase plane of CSMC for step command.

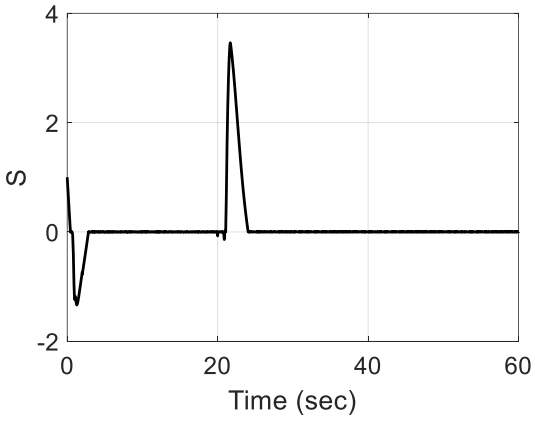

Figure 18. Surface curve of CSMC for step command.

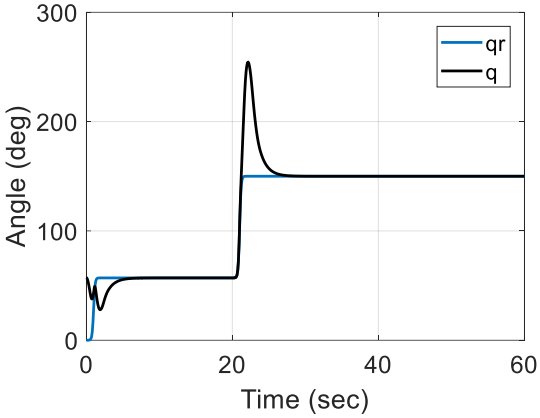

Figure 19. Angle response of SOSMC for step command.

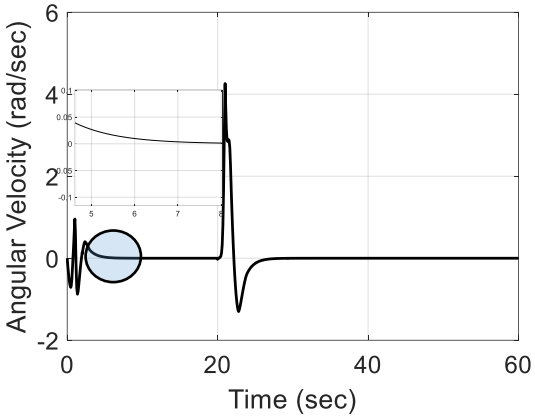

Figure 20. Angular velocity response of SOSMC for step command.

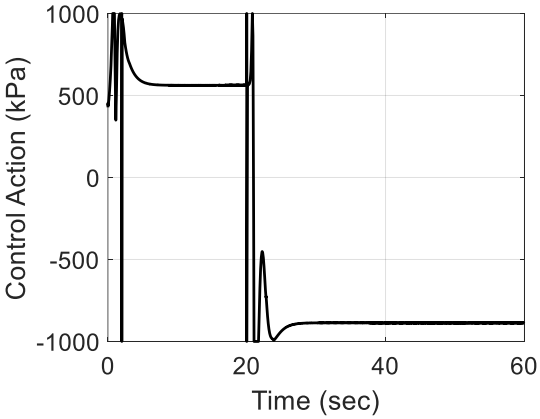

Figure 21. Control action of SOSMC for step command.

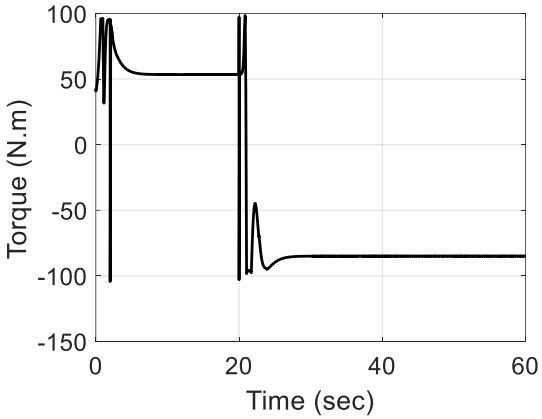

Figure 22. Torque of SOSMC for step command.

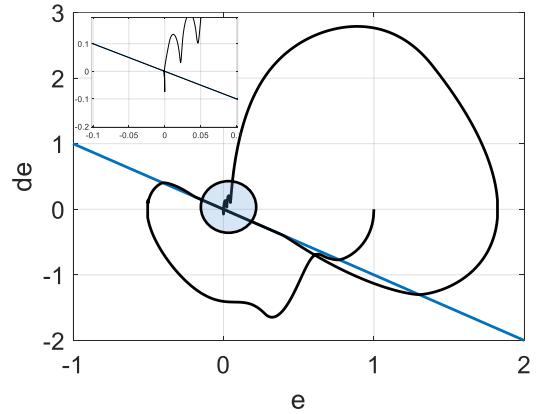

Figure 23. Phase plane of SOSMC for step command.

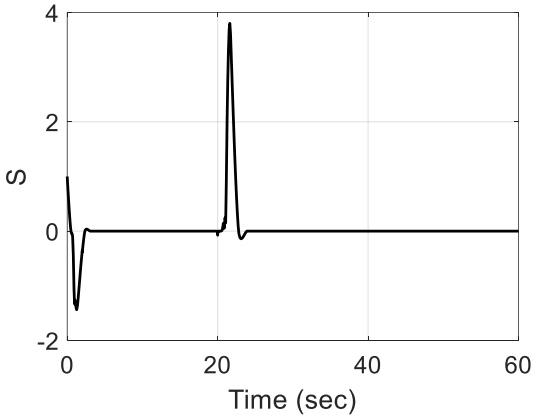

Figure 24. Surface curve of SOSMC for step command.

Table 1. Bicep and tricep PAM parameters, **Repperger, et al., 1998.**

Parameter	Inflated	Deflated
k_{1i}	1.6	3.6
k_{2i}	-10.9	-20.7
k_{3i}	27.1	47.23
b_{1i}	0.04	0.12
b_{2i}	-1.3	-2.49
b_{3i}	12.6	14.48

Table 2. The robotic arm parameters (assumed).

Parameter	value	unit
m	20	Kg
l	0.5	m
I	1.667	$Kg.m^2$
g	9.81	m/s^2
r	0.05	m
P_{0b}	400	kPa
P_{0t}	400	kPa

Table 3. The total system parameters (calculated from Eq. 14)

Parameter	$\dot{q} > 0$	$\dot{q} < 0$
δ_1	-0.00012581	-0.00012581
δ_2	-0.0002257	0.0002257
δ_3	-0.033579	-0.033579
δ_4	-1.9355e-07	-1.9355e-07
δ_5	-2.879e-05	2.879e-05
δ_6	-0.013103	-0.013103
δ_7	-18.9871	-18.9871
δ_8	0.015115	-0.015115
b	0.019355	0.019355